Systems & Control Transactions

Original Research Article
Peer Reviewed Conference Proceeding
ESCAPE 36 - European Symposium on Computer Aided Process Engineering
Sheffield, UK. 21-24 June 2026

PSE PRESS

Active-Constraint Regions and Power Distribution in Multi-Stack PEM Water Electrolysis Systems

Marius Fredriksen[a], Johannes Jäschke[a]*

[a] Norwegian University of Science and Technology, Department of Chemical Engineering, Trondheim, Norway
* Corresponding Author: johannes.jaschke@ntnu.no

ABSTRACT

Multi-stack proton exchange membrane (PEM) water electrolysis systems are increasingly deployed to improve the scalability and flexibility of green hydrogen production. However, sharing balance-of-plant equipment introduces coupling between stacks, and differences in stack performance increase the complexity of plantwide operation. In particular, non-identical efficiencies and safety constraints, such as hydrogen-to-oxygen (HTO) ratio limits, can render single-stack or equal-power-sharing control strategies suboptimal. In this work, the steady-state optimal operating regime of a two-stack PEM electrolysis system is characterized using a plantwide optimization approach and active constraint mapping over a range of system power loads. Performance differences between the stacks are represented through variations in Faraday efficiency to emulate simplified degradation. For identical stacks, the system behaves similarly to a single large electrolyzer, where equal power distribution is optimal, and the active constraint regions closely resemble those of a single-stack system. As the stack performance differences increase, the optimal power distribution becomes asymmetric, with the more efficient stack preferentially loaded. However, HTO safety constraints in the degraded stack may limit the utilization of the more efficient stack and introduce additional active constraint regions, resulting in more complex operating regimes.

Keywords: Hydrogen, Energy Management, Process Optimization, PEM Electrolysis, Active Constraint Regions

INTRODUCTION

Hydrogen is expected to play a key role in decarbonization, and the development of large-scale, safe, and efficient production technologies is therefore required to meet zero-emission targets. Proton exchange membrane (PEM) water electrolysis is particularly attractive due to its high efficiency, fast dynamics, and suitability for intermittent renewable power. To reach industrially relevant capacities, modern PEM systems employ multiple stacks operating in parallel, often connected through a shared balance of plant (BoP). Such multi-stack configurations improve scalability and cost-effectiveness at high power loads compared to single-stack systems [2]. However, parallel stacks significantly increase system complexity and make plantwide operation more challenging due to coupling effects.

Despite this, most studies on PEM electrolysis focus primarily on single-stack performance. While several works have investigated power distribution strategies for multi-fuel-cell systems, considerably less research has addressed multi-stack PEM water electrolysis [2]. Among the existing studies, Xinyu et al. [11] proposed a daisy-chain power-distribution strategy, Cheng et al. [2] developed a power-adaptive fuzzy PID approach to improve load flexibility, and Guo et al. [5] introduced a rule-based strategy for hybrid PEM–alkaline systems utilizing the hydrogen-to-oxygen (HTO) impurity ratio.

Furthermore, due to manufacturing tolerances, aging, and thermal differences, individual stacks may exhibit different efficiencies. As a result, equal power sharing can be suboptimal and, in the worst case, violate operational or safety constraints. These performance differences should therefore be considered when determining power allocation among stacks [11].

In this work, we determine the steady-state optimal operating regime of a two-stack PEM electrolyzer system by solving a plantwide optimization problem and mapping the resulting active constraint regions across a range of power inputs. This analysis reveals how power should be

distributed between two PEM stacks operating in parallel and how differences in Faraday efficiency affect the optimal power allocation. The goal is to quantify how differences in stack performance affect the system's operating conditions and to provide a foundation for future control development.

METHODOLOGY

In this section, we briefly describe the two-stack PEM electrolysis system, the underlying process model, and the optimization framework used to determine the optimal power allocation and corresponding active constraint regions.

Case study and system layout

The system consists of two 60 kW PEM water electrolyzer stacks operating in parallel. Each stack has its own heat exchanger for temperature regulation and a dedicated power converter. The stacks share common BoP equipment, including two gas–liquid separators, a deionized water buffer tank, four pumps, four valves, and a hydrogen compressor. The piping is neglected as its effect on the steady-state operating conditions is negligible. The overall system layout is shown in Figure 1.

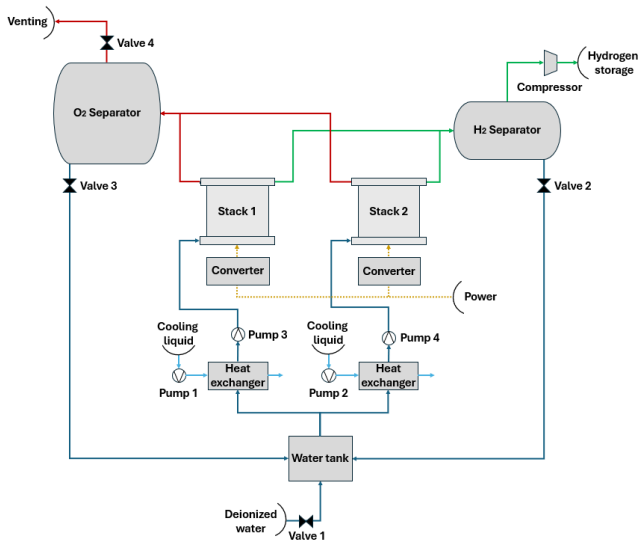

Figure 1. System layout of the two-stack PEM water electrolysis system with parallel stacks and shared balance-of-plant equipment.

Deionized water from the buffer tank is cooled in the heat exchangers and then supplied to the stacks, where it is electrolyzed to produce hydrogen and oxygen. The produced gases are subsequently separated from the liquid water in the gas–liquid separators, after which the oxygen is vented, and the hydrogen is compressed for downstream treatment. Finally, the remaining water is recycled back to the buffer tank.

Sharing separators introduces coupling between the stacks and additional operational constraints. In particular, both stacks must operate at similar pressures, limiting independent adjustment of membrane pressure gradients for gas crossover control. Furthermore, the HTO ratio measured at the separator does not directly reflect the HTO within each stack; therefore, stack-level HTO values must be estimated.

Process model description

The PEM electrolysis system model is adopted from our previous work [4], which combines electrochemical, thermal, and mass-transport stack submodels with standard mass and energy balances for the BoP equipment. For brevity, only the relations most relevant to the steady-state optimization are summarized in this work; for a more detailed model description, we refer to [4].

Electrochemical relations

The Stack performance is described using the electrochemical submodel that relates cell voltage (V_{cell}) to the current density (i_{el}) at a given power. The cell voltage is expressed as the sum of the reversible potential (V_{rev}), and the ohmic (V_{ohm}), activation (V_{act}), and concentration (V_{con}) overpotentials,

$$V_{cell} = V_{rev} + V_{ohm} + V_{act} + V_{con}, \tag{1}$$

where the reversible voltage represents the thermodynamic minimum energy required to drive the reaction, and the remaining terms account for resistive, kinetic, and mass-transport losses. The reversible potential is computed from the Gibbs free energy and corrected for pressure effects using the Nernst equation. Ohmic losses are estimated using an empirical membrane resistance correlation for Nafion 117, while activation and concentration losses are described using Tafel-type kinetics [1, 3, 8].

Faraday efficiency and degradation

Hydrogen production is calculated using Faraday's law of electrolysis. To represent performance differences between stacks, a Faraday efficiency factor (η_F) is introduced as a multiplicative term on the electrochemical gas generation rates,

$$\dot{n}_{\mathrm{gen},H_2} = \frac{i_{\mathrm{el}}A}{zF}\eta_F, \dot{n}_{\mathrm{gen},O_2} = \frac{i_{\mathrm{el}}A}{2zF}\eta_F. \tag{2}$$

A is the active membrane area, z is the number of electrons transferred, and F is the Faraday's constant [3]. Values $\eta_F < 1$ represent parasitic charge consumption (e.g., crossover-related recombination and other side currents), resulting in reduced hydrogen production per unit current. The associated electrical losses are assumed to be dissipated as heat. However, since this study focuses primarily on HTO constraints and steady-state power allocation, additional heat generation is neglected for simplicity.

HTO ratio and gas solubility

The HTO ratio is defined as the volumetric fraction of hydrogen relative to oxygen. Assuming ideal-gas behavior, this ratio can be estimated directly from the gas-phase composition,

$$HTO = \frac{V_{H_2}}{V_{O_2}} = \frac{y_{H_2}}{y_{O_2}}, \tag{3}$$

where V is the gas volume and y the gas-phase mole fraction.

The gas inventories in the separators are determined by subtracting dissolved gases from the total species inventories. The amount of dissolved gases is estimated using Henry's law with temperature-dependent solubility constants (H) obtained from Sander [9],

$$H = H_0 \cdot \exp\left(B\left(\frac{1}{T} - \frac{1}{T_0}\right)\right). \tag{4}$$

H_0 is the Henry constant at the reference temperature $T_0 = 298.15$ K, T is the stack/separator temperature, and B is an empirical temperature parameter. Gas solubility within the membrane is described using the correlations presented by Afshari et al. [1] and is assumed constant.

For simplicity, the stack-level HTO is computed using the total hydrogen and oxygen inventories. Due to oxygen's higher solubility in water, HTO values are slightly lower inside the stacks than in the separators, particularly at low pressure and temperature.

Compression and pump work

Compression and pumping contribute to the total system power consumption and therefore influence the optimal operating regime. Hydrogen leaving the cathode is compressed to 30 barg for downstream handling, while liquid water and coolant are circulated through the stacks and heat exchangers by pumps. Including these auxiliary loads allows the optimization to capture the trade-off between electrochemical stack efficiency and mechanical energy requirements for compression and circulation.

The compressor is modeled assuming multistage compression with intercooling, resulting in approximately isothermal behavior. The required compression work is estimated as,

$$W_c = \frac{\dot{n}_{H_2} R T_{\text{sep}}}{\eta_c} \ln\left(\frac{P_{\text{storage}}}{P_{\text{sep}}}\right), \tag{5}$$

where $\dot{n}_{H_2}$ is the hydrogen molar flow rate, T_{sep} is the separator temperature, P_{storage} and P_{sep} denote the storage and separator pressures, and η_c is the compressor efficiency (80%).

The pump work is approximated by,

$$W_p = \frac{\dot{m}}{\rho} \frac{(P_{\text{final}} - P_{\text{initial}})}{\eta_p}. \tag{6}$$

$\dot{m}$ is the mass flow rate, ρ is the liquid density, and η_p is the pump efficiency (75%).

Steady state optimization formulation

To determine the optimal operating policy, a steady-state optimization problem is solved over a range of system power inputs. The total electrical power is treated as an external disturbance representing the available power supply, while the internal power distribution between stacks is optimized. For each load level, the objective is to maximize the hydrogen output subject to the process model and operational constraints.

$$\begin{aligned} \max_{\text{MVs}} \quad & \dot{n}_{H_2} \\ s.t. \quad & \text{Process model equations} \\ & \text{Operational constraints} \end{aligned} \tag{7}$$

The manipulated variables (MVs) correspond to the available actuators in the system, namely valves, pumps, power converters, and the hydrogen compressor. With the liquid inventories in the separators and buffer tank regulated by local control loops and the feedwater flow rates fixed, five MVs remain for the optimizer. These are the oxygen outlet valve (z_4), the compressor work (W_c), the work of the two cooling liquid pumps (W_{p3}, W_{p4}), and the stack power distribution factor (α), which determines the fraction of total power supplied to each stack,

$$MVs = [z_4, W_c, W_{p3}, W_{p4}, \alpha]. \tag{8}$$

Operational limits are imposed on stack pressure, temperature, and the HTO ratio to ensure safe operation. Although the lower explosion limit of hydrogen in oxygen is approximately 4 vol.%, the HTO constraint is conservatively set to 2 vol.% to provide a safety margin. Upper bounds on stack pressure and temperature are adopted from Crespi et al. [3]. Additional constraints are imposed on minimum stack power (5% of nominal load) and cooling liquid flow rates to ensure physically feasible operation. The resulting bounds are summarized in Table 1.

Table 1: PEM system operating constraints.

Condition	Lower bound	Upper bound
Stack power	3 kW	60 kW
Anode pressure	0.2 barg	2.7 barg
Cathode pressure	0.2 barg	30 barg
Temperature	10 °C	60 °C
Cooling liquid	0 mol/s	15 mol/s
HTO ratio	0 vol.%	2 vol.%

The optimization problem is solved for 120 evenly spaced values of total power input, ranging from 6 to 120 kW. For each operating point, all constraints are scaled between 0 and 1 and used to identify the corresponding active constraint region. A constraint is considered active when its scaled value reaches either 0 for the lower limit or 1 for the upper limit. This procedure is repeated for multiple Faraday efficiency scenarios to evaluate the

impact of stack degradation and performance differences.

The steady-state optimization problem is implemented in Julia (v1.9.3) using JuMP (v1.29.0) [7]. The resulting problem is solved with the Ipopt (v1.11.0) interior-point solver [10], using the HSL MA57 linear solver [6].

RESULTS AND DISCUSSION

To evaluate the impact of stack performance differences on optimal operation, active constraint regions are analyzed for three efficiency scenarios. In Scenario 1, both stacks operate with identical Faraday efficiencies of 100%. In Scenarios 2–3, the efficiency of Stack 2 is reduced to 90% and 80%, respectively, while Stack 1 remains at nominal performance. Although these reductions are more severe for the Faraday efficiency than typically observed in practice, they are intentionally introduced to clearly illustrate how stack mismatch influences the optimal power distribution and operating regime. The considered scenarios and the corresponding number of active constraint regions are summarized in Table 2.

Table 2: Faraday efficiency scenarios for Stack 2 and the corresponding number of active constraint regions. The efficiency of Stack 1 is fixed at 100%.

Scenario	Stack 2 Faraday efficiency [%]	Active constraint regions [#]
1	100	2
2	90	5
3	80	6

Scenario 1 – Identical stacks

The optimal operating regime, active constraint regions, and corresponding power distribution for Scenario 1 are shown in Figure 2.

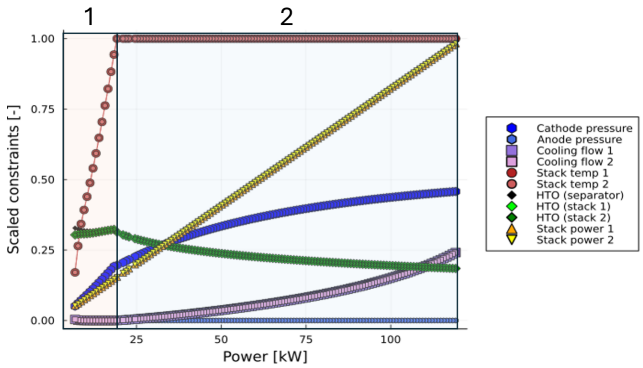

Figure 2. Optimal operating regime and active constraint regions for Scenario 1.

When both stacks have identical efficiencies, the optimizer distributes the power evenly between them. This is expected, since operating each stack at a lower individual power load improves hydrogen production per unit of power. Consequently, the two-stack system behaves similarly to a single larger stack.

At low loads, the stack temperatures increase rapidly with power until the upper temperature constraint becomes active at approximately 20 kW. Because higher temperatures improve electrochemical efficiency, the optimizer keeps the cooling flow rates at their lower bounds until the maximum temperatures are reached.

The anode pressure remains at its lower bound across the entire operating range due to the small efficiency penalty associated with elevated pressures. In contrast, the cathode pressure gradually increases with load. This behavior arises because the optimizer utilizes the stack pressure to partially compress the produced hydrogen, thereby reducing the work required by the downstream compressor. Although in-stack compression is generally more energetically favorable than mechanical compression, the compressor is modeled as a highly efficient isothermal unit. As a result, the optimizer prefers using both the compressor and the stack for compression. However, a less efficient compressor would likely result in higher optimal cathode pressures.

The HTO constraint remains inactive throughout this scenario. This is partly due to the low pressure gradients at small loads and partly due to the equal power distribution between the stacks, which results in similar crossover behavior. At very low power levels, the separator HTO is slightly higher than the stack HTO. This difference arises because the stack HTO is computed from the total gas inventories, whereas the separator measurement excludes gases dissolved in the liquid phase.

As both stacks operate under identical conditions, the active constraint regions closely resemble those of a single-stack system [4]. One of the main differences is that the single-stack system exhibits a slightly higher anode pressure at high loads. In the multi-stack configuration, however, increasing the anode pressure requires additional pump work due to the extra feedwater pump, making such operation less favorable.

Consequently, two active constraint regions are identified for the multi-stack system. In Region 1, the temperature constraints are inactive, and the cooling liquid flow rates remain at their lower bounds. As the load increases and the upper temperature constraints become active, the system transitions to Region 2, where additional cooling is required to maintain safe operation. Both regions have two degrees of freedom (DoFs), defined as the number of MVs minus the number of active constraints.

Scenario 2 – Stack 2 at 90 %

In Scenario 2, the Faraday efficiency of Stack 2 is reduced to 90%, introducing asymmetry between the two stacks. The optimal operating regime, active constraint

regions, and power distribution are shown in Figure 3.

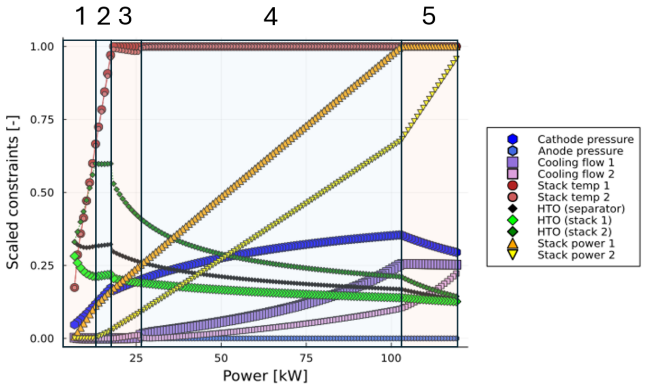

Figure 3. Optimal operating regime and active constraint regions for Scenario 2.

Stack 1 is more efficient than Stack 2, therefore the optimizer allocates a larger share of the power load to this electrolyzer. This behavior is expected and consistent with prior work recommending preferential use of the most efficient stack [11].

The HTO ratio of Stack 2 becomes significantly higher than that of Stack 1 at low loads. This occurs because reduced Faraday efficiency lowers oxygen production, thereby reducing hydrogen crossover dilution. At low loads, the HTO in Stack 2 increases rapidly until additional power is allocated to the stack, demonstrating a clear coupling between stack loading and the HTO ratio.

The temperature behavior largely follows Scenario 1. However, Stack 2 operates slightly below its upper temperature limit when Stack 1 reaches its constraint. Since Stack 2 contributes less to the overall hydrogen production in this region, operating at a lower temperature incurs a relatively minor efficiency penalty while slightly reducing downstream compression work. The optimizer also concentrates cooling on Stack 2, effectively allowing one cooling circuit to assist both stacks by overcooling the less efficient electrolyzer.

The cathode pressure remains inactive throughout the operating range and follows the same trend as in Scenario 1, but at lower absolute values. The maximum cathode pressure decreases from 14.84 bar in Scenario 1 to 11.75 bar, while the anode pressure remains fixed at its lower bound.

Scenario 2 has five active constraint regions. Regions 1–2 resemble Region 1 from Scenario 1, where the temperature constraints are inactive. However, in Region 1, Stack 2 operates at minimum power, while in Region 2, its load gradually starts increasing. In Region 3, the temperature constraint on Stack 1 becomes active, and Stack 2 is slightly overcooled. In Region 4, the temperature constraint on Stack 2 also becomes active. Finally, in Region 5, Stack 1 reaches its maximum allowable power, limiting further redistribution. Regions 2–4 have two DoFs, while Regions 1 and 5 have one DoF.

Scenario 3- Stack 2 at 80 %

In Scenario 3, the Faraday efficiency of Stack 2 is reduced to 80%, further increasing the performance mismatch between the two stacks. The resulting optimal operating regime, active constraint regions, and power distribution are shown in Figure 4.

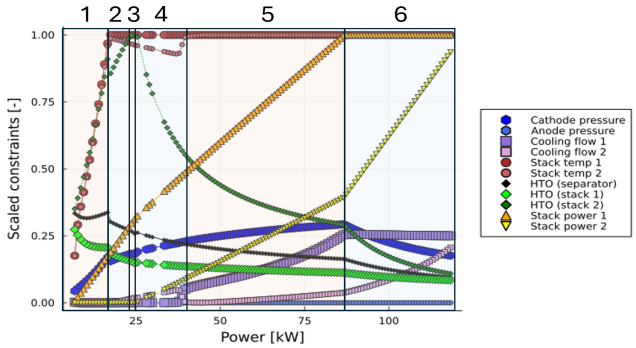

Figure 4. Optimal operating regime and active constraint regions for Scenario 3.

The overall behavior follows the same trends observed in Scenario 2, but with more pronounced asymmetry. The optimizer allocates an even larger fraction of the total load to Stack 1, causing Stack 2 to operate at its minimum power over a wider range of low system loads, while Stack 1 remains at its upper power limit for a larger portion of the high-load region.

As a result of this extended low-power operation, the HTO ratio in Stack 2 increases and reaches its upper constraint, which becomes active over a small portion of the operating range. When the HTO limit is reached, the cathode pressure stagnates slightly before the power load of Stack 2 begins to increase. This behavior indicates a clear relationship between the stack HTO, the pressure gradient, and the power load, where either the stack power must be increased or the cathode–anode pressure gradient reduced to maintain the HTO ratio of the degraded stack within safe limits.

Consistent with the reduced utilization of Stack 2, its operating temperature decreases further compared to Scenario 2. The cathode pressure continues to decrease, with the maximum dropping to 9.92 bar, while the anode pressure remains at its lower bound.

The increased stack asymmetry adds another active constraint region as the HTO limit of Stack 2 becomes active, yielding six active constraint regions in Scenario 3. In Region 1, Stack 2 operates at minimum power, with the anode pressure and both coolant flow rates at their lower bounds. In Region 2, the temperature constraint of Stack 1 becomes active, and the coolant flow of Stack 2 leaves its bound. In Region 3, the HTO constraint for Stack 2 becomes active, and it subsequently relaxes in

Region 4 as the lower power limit for Stack 2 becomes inactive. In Region 5, both temperature constraints are active, and in Region 6, Stack 1 reaches its maximum power limit. Regions 1, 2, 3, and 6 have one DoF, while Regions 4 and 5 have two.

CONCLUSION AND FUTURE WORK

This work investigates how differences in stack performance affect the optimal operating regime and active constraint regions of a two-stack PEM water electrolysis system. For identical stacks, the plant behaves similarly to a large single-stack system, and equal power allocation remains optimal across the entire operating region.

As performance differences are introduced, the optimal allocation becomes asymmetric, with the more efficient stack preferentially loaded. However, this utilization is restricted by safety constraints, particularly the HTO limit in the degraded stack. To maintain safe operation, the system must balance power allocation and pressure levels. This coupling between HTO, pressure, and power leads to additional active constraint regions, fragmenting the operating space and increasing the complexity of the optimal operating policy. These findings highlight the importance of accounting for stack asymmetry when designing control strategies for multi-stack systems.

Future work will use the identified operating regimes and active constraint regions to develop appropriate control structures for multi-stack PEM electrolysis systems using dynamic plant models. Additionally, the impact of extending the framework to systems with more stacks will be investigated.

ACKNOWLEDGEMENTS

This work was supported by the HYDROGENi Research Centre (hydrogeni.no) under the Norwegian research program FMETEKN. The authors acknowledge the industry partners in HYDROGENi for their contributions and the Research Council of Norway (project no. 333118).

DECLARATION OF GENERATIVE AI AND AI-ASSISTED TECHNOLOGIES IN THE WRITING PROCESS

During the preparation of this work, the authors used generative AI tools (ChatGPT and GitHub Copilot) to assist with phrasing, language improvement, and to generate code suggestions. After using these tools, the authors reviewed and edited the content as needed and take full responsibility for the publication's content.

REFERENCES

1. Afshari E, Khodabakhsh S, Jahantigh N, Toghyani S. Performance assessment of gas crossover phenomenon and water transport mechanism in high pressure PEM electrolyzer. International Journal of Hydrogen Energy 46:11029-11040 (2021). https://doi.org/10.1016/j.ijhydene.2020.10.180
2. Cheng K, He S, Hu B. Power adaptive control strategy for multi-stack PEM photovoltaic hydrogen systems considering electrolysis unit efficiency and hydrogen production rate. Sustainable Energy Technologies and Assessments 75:104200 (2025). https://doi.org/10.1016/j.seta.2025.104200
3. Crespi E, Guandalini G, Mastropasqua L, Campanari S, Brouwer J. Experimental and theoretical evaluation of a 60 kw PEM electrolysis system for flexible dynamic operation. Energy Conversion and Management 277:116622 (2023). https://doi.org/10.1016/j.enconman.2022.116622
4. Fredriksen M, J?schke J. Advanced regulatory control structure for proton exchange membrane water electrolysis systems. Systems and Control Transactions 4:1011-1016 (2025). https://doi.org/10.69997/sct.130330
5. Guo Y, Qi P, Zhang Q, Li M, Liu J, Sun H. Control strategy for hydrogen production system using hto-based hybrid electrolyzers. Energy Reports 13:2354-2364 (2025). https://doi.org/10.1016/j.egyr.2025.01.012
6. HSL. A collection of Fortran codes for large scale scientific computation. http://www.hsl.rl.ac.uk/
7. Lubin M, Dowson O, Garcia JD, Huchette J, Legat B, Vielma JP. Jump 1.0: recent improvements to a modeling language for mathematical optimization. Math. Prog. Comp. 15:581-589 (2023). https://doi.org/10.1007/s12532-023-00239-3
8. Ojong ET, Kwan JTH, Nouri-Khorasani A, Bonakdarpour A, Wilkinson DP, Smolinka T. Development of an experimentally validated semi-empirical fully-coupled performance model of a PEM electrolysis cell with a 3-D structured porous transport layer. International Journal of Hydrogen Energy 42:25831-25847 (2017). https://doi.org/10.1016/j.ijhydene.2017.08.183
9. Sander R. Compilation of henry's law constants (version 5.0.0) for water as solvent. Atmos. Chem. Phys. 23:10901-12440 (2023). https://doi.org/10.5194/acp-23-10901-2023
10. Wächter A, Biegler LT. On the implementation of an interior-point filter line-search algorithm for large-scale nonlinear programming. Math. Program. 106:25-57 (2005). https://doi.org/10.1007/s10107-004-0559-y
11. Xinyu L, Banghua D, Bo Z, Lqilei Z, & Changjun X. Design and control of wind-hydrogen coupled

system based on chain distribution strategy [J]. Journal of Solar Energy, 43(06), 05-413. (2022)